Available online at www.sciencedirect.com
SCIENCE DIRECT
Computer Coupling of Phase Diagrams and Thermochemistry 30 (2006) 216–224
www.elsevier.com/locate/calphad

Models for the determination of kinetic phase diagrams and kinetic phase separation domains

J.H. Los[a,*], M. van den Heuvel[a], W.J.P. van Enckevort[a], E. Vlieg[a], H.A.J. Oonk[b], M. Matovic[b], J.C. van Miltenburg[b]

[a] *IMM Laboratory of Solid State Chemistry, Radboud University Nijmegen, Toernooiveld, 6525 ED Nijmegen, The Netherlands*
[b] *Chemical Thermodynamics Group, Debeye Institute, Utrecht University, Padualaan 8, 3584 CH Utrecht, The Netherlands*

Received 15 September 2005; received in revised form 28 November 2005; accepted 7 December 2005
Available online 4 January 2006

Abstract

Several theoretical models for the determination of kinetic phase diagrams for solid solution growth from the liquid phase are presented and compared to each other. These models include a Monte Carlo simulation model, used as a reference model, a previously defined analytical model, based on linear non-equilibrium thermodynamics, and a new model, rooted in the kinetics at kink sites.

All models have in common that the composition of the growing solid phase tends to the liquid phase composition for increasing undercooling, enhancing mixing even for systems with a strong tendency to phase separation. However, depending on the system parameters considerable quantitative differences can occur between the results from the model based on non-equilibrium thermodynamics and the MC model. Instead, the new model follows very well the trends of the MC simulations, both for well-mixing systems and for phase separating systems.

For phase separating systems the analytical models predict kinetic phase separation domains, zones in the kinetic phase diagram yielding steady state growth of more than one solid phase with different compositions. According to MC simulations such domains in phase space correspond to domain formation in real space. Also in this case the new model is consistent with the MC results.

1. Introduction

In certain cases it can take a very long time for a system to reach its equilibrium state, the state with minimal Gibbs free energy, represented graphically in the equilibrium phase diagram. This holds particularly for mixed solid phases, here meant as solid solutions, due to the very low diffusion rate in solids, which makes built-in inhomogeneities persist for very long times. The extent of these deviations from equilibrium will depend on the history of the system, especially on the kinetics during the growth, which depend on the growth conditions and also on the scale of the system. The occurrence of such deviations is well known and has also been demonstrated experimentally [1–3]. Theoretically, the extent of the deviations was investigated on the basis of a kinetic crystallization model [4,5], both for well-mixing systems [4] and for systems showing phase separation [5].

The mentioned non-equilibrium states, or metastable states, complicate the determination of equilibrium phase diagrams, requiring efforts to prepare mixtures with a high degree of homogeneity [6,7]. It has also led to the method implemented in the software program LIQFIT for the determination of excess parameters by fitting experimental data, which is based on fitting only the liquidus points and not the solidus points which are considered unreliable [8]. In Ref. [3] the complications due to non-equilibrium states are tackled in a different way for slow crystallization processes performed in an adiabatic calorimeter by dropping the assumption of total equilibrium and replacing it by assuming equilibrium between the liquid phase and only the surface of the solid phase during growth. In this way both enthalpy and entropy excess parameters were successfully derived from experimental cooling curves. However, this method can only be applied for slow crystallization, typical for adiabatic calorimetry, and cannot be applied for conditions away from near-equilibrium, which often occur in e.g. differential scanning calorimetry (DSC). An appropriate interpretation at such conditions

* Corresponding author. Tel.: +31 243652363; fax: +31 243653067.
E-mail address: j.los@science.ru.nl (J.H. Los).

0364-5916/$ - see front matter © 2005 Elsevier Ltd. All rights reserved.
doi:10.1016/j.calphad.2005.12.002

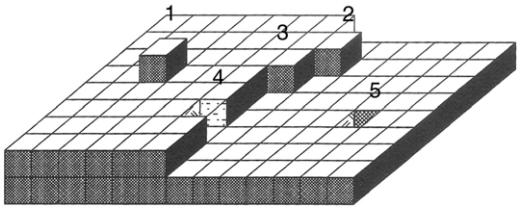

Fig. 1. Schematic illustration of the Kossel model for crystal growth. Reactive particles at the surface may have one, two, three, four or five bonds. A particle with three bonds is called a kink particle. Kink sites play an important role in the growth process.

requires a kinetic modelling of the crystallization process, with first of all knowledge of the kinetic phase diagrams (KPDs) of the issued mixture. KPDs, or non-equilibrium phase diagrams, provide the composition of a growing solid phase as a function of the liquid composition and of the undercooling at the solidification front.

Experimentally, the determination of KPDs is a complicated task, mostly due to the difficulty of measuring the precise conditions at the surface, in particular the temperature and the liquid composition. This difficulty mainly originates from diffusion limitation, i.e. the finiteness in the speed of transport of mass and heat which makes the conditions at the surface different from the bulk properties and change in time, particularly for fast crystal growth. Here theory can play an important role to bridge the gap between what can be measured with reasonable effort and the desired data.

In the past, binary crystal growth has been modelled by Monte Carlo (MC) simulations [10,11] based on the Kossel model [12,13] (see Fig. 1). These simulation models have also been the inspiration for the formulation of models consisting of kinetic equations [14,15], describing the growth kinetics and segregation within certain approximations. Other works on kinetic segregation [16–20] were inspired by the observed high doping concentration in semiconductor materials after rapid crystallisation [21–23]. In the analytical models proposed in these works the kinetic segregation coefficient k is expressed as a function of the known equilibrium segregation coefficients k_{eq} and the observed crystal growth velocity, such that k becomes equal to k_{eq} when the growth rate tends to zero, i.e. at equilibrium. These models take into account the diffusion limitation in the liquid phase, but they do not include the details of the surface kinetics. Recently, new models for the interface kinetics and segregation for the growth of binary crystals, also based on the Kossel model, have appeared [24–26]. These models distinguish between the segregation for different types of sites (i.e. kink, step, terrace and bulk sites), but are restricted to systems with ideal mixing properties.

In previous work we have shown examples of KPDs [5, 27], calculated using a rather simple analytical model based on linear non-equilibrium thermodynamics, the so-called linear kinetic segregation (LKS) model. This model is defined in terms of the thermodynamic properties of the system, including the pure component properties and the mixing properties, and is not restricted to the ideal mixing case. In fact, for mixed systems with a sufficiently strong tendency to phase separation it can predict kinetic phase separation, indicating the possibility of the simultaneous growth of more than one solid phase with different compositions from the same liquid phase. This property gives rise to so-called kinetic phase separation domains KPSDs, zones in a kinetic phase diagram where kinetic phase separation occurs.

In this work we will test the LKS model by comparing its predictions with the results of MC simulations based on the Kossel model, both for well-mixing systems and for phase separating systems. We also introduce a second analytical model, which is also compared with the MC results. Thereby we will concentrate on the kinetic segregation for a given liquid phase composition and isothermal conditions at the surface. Thus, here we will not consider the effects of transport limitations in the liquid phase, involving relations between the liquid phase properties at the surface and those in the bulk. This coupling of the interface segregation with mass and heat transport has recently been treated elsewhere [9].

In the next section, we describe the binary Kossel model. Section 3 contains a description of the analytical models. We first briefly describe the previously presented LKS model and then present the new model. In Section 4 we present kinetic phase diagrams (KPDs) for several model systems, comparing the predictions of the analytical models with the results from MC simulations. Section 5 deals with phase separation systems, giving rise to kinetic phase separation domains (KPSDs) according to the analytical models. Calculated KPSDs are presented and a comparison with MC simulations is made.

2. Binary Kossel model

The Kossel model is a Monte Carlo simulation model for crystal growth on a simple cubic lattice, originally developed for pure crystals [12]. An illustration of a Kossel surface is given in Fig. 1. Particles, represented as cubes, can attach and detach at the surface with certain probabilities, derived from thermodynamic considerations.

In principle the extension of the Kossel model to a binary system is straightforward, but requires a link with the thermodynamic pure component properties and mixing properties. Such a link can be established as follows.

In this work, we will assume systems where the difference in the excess mixing energy between the liquid and the solid phase is described by one single parameter, $\Delta\mathcal{U}_0^{\mathrm{exc}} \equiv \mathcal{U}_0^{l,\mathrm{exc}} - \mathcal{U}_0^{s,\mathrm{exc}}$. Hence, we assume that the difference in internal energy of the liquid, U^l, and the solid phase, U^s, of equal mole fractions $x_i^l = x_i^s$ $(i = 1, 2)$, is given by:

$$\Delta U = U^l - U^s = x_1^s \Delta U_1 + x_2^s \Delta U_2 + x_1^s x_2^s \Delta\mathcal{U}_0^{\mathrm{exc}} \tag{1}$$

where ΔU_1 and ΔU_2 are the melting energies of the pure components 1 and 2 respectively. Furthermore, we will assume regular solutions, i.e. the excess entropy is zero in both the liquid and the solid phase. Such 'simple' systems show all the relevant phenomena for the present study, including phase separation. For convenience, without further loss of generality, the mixing in the liquid phase is taken to be ideal, implying $\Delta\mathcal{U}_0^{\mathrm{exc}} = -\mathcal{U}_0^{s,\mathrm{exc}}$, and the liquid energy level is chosen to be zero for any composition so that $\Delta U = -U^s$.

The exact bulk energy of the binary Kossel crystal (BKM) per particle can be written as:

$$U^s_{\mathrm{BKM}} = -\frac{Z}{2}\left(x^s_{11}\phi_{11} + x^s_{22}\phi_{22} + x^s_{12}\phi_{12}\right) \tag{2}$$

where $Z = 6$ is the coordination, ϕ_{ij} is the bond energy between particles of type i and j ($i, j = 1, 2$) and x_{ij} is the fraction of ij-bonds in the bulk crystal. A relation between these bond energies and the thermodynamic parameters ΔU_i and $\Delta \mathcal{U}^{\mathrm{exc}}_0$ can be derived applying a mean field (MF) approximation. Within the MF approximation it holds:

$$x^s_{ii} = (x^s_i)^2 \quad (i = 1, 2) \quad \text{and} \quad x^s_{12} = 2x^s_1 x^s_2 \tag{3}$$

where x^s_i is the bulk mole fraction of component i. Substitution of Eq. (3) into Eq. (2) and using $x^s_1 = 1 - x^s_2$ leads to the following mean field expression for the energy:

$$U^s_{\mathrm{MF}} = -\frac{Z}{2}\left(x^s_1\phi_{11} + x^s_2\phi_{22} + 2x^s_1 x^s_2\phi^{\mathrm{exc}}\right) \tag{4}$$

where ϕ^{exc} is the excess bond energy defined by:

$$\phi^{\mathrm{exc}} = \phi_{12} - \frac{1}{2}\left(\phi_{11} + \phi_{22}\right). \tag{5}$$

Then, combining Eqs. (4) and (1) leads to:

$$\phi_{ii} = \frac{2\Delta U_i}{Z}\ (i = 1, 2) \quad \text{and} \quad \phi_{12} = \frac{\Delta U_1 + \Delta U_2 - \mathcal{U}^{s,\mathrm{exc}}_0}{Z}. \tag{6}$$

The Monte Carlo algorithm consists of a large number of events, each event being either the attachment or the detachment of a particle at the surface, respecting the solid on solid (SOS) condition [12]. The change in the free energy $\tilde{F}$, not including the ideal mixing entropy term, for a selected event, being the attachment or the detachment of a particle of type i at a given surface site, is given by:

$$\Delta\tilde{F}_{ev,i} = \Delta U_{ev,i} - T\Delta\tilde{S}_{ev,i} \tag{7}$$

where $\Delta U_{ev,i}$ and $\Delta\tilde{S}_{ev,i}$ are the changes in the internal energy and the vibrational entropy respectively, and T the absolute temperature. For the detachment of a particle of type i with n_1 neighbours of type 1 and n_2 neighbours of type 2, ΔU_{ev} is taken equal to the energy of the broken bonds:

$$\Delta U_{ev,i} = n_1\phi_{i1} + n_2\phi_{i2} \tag{8}$$

whereas the entropy change $\Delta\tilde{S}_{ev,i}$ is taken to be the pure component dissolution entropy, ΔS_i, of component i:

$$\Delta\tilde{S}_{ev,i} = \Delta S_i = \frac{\Delta U_i}{T_i} = \frac{3\phi_{ii}}{T_i} \tag{9}$$

where T_i the melting temperature of the pure component i. According to the detailed balance principle, which is supposed to hold for the individual microscopic events in (non-extreme) non-equilibrium situations as well, the ratio between the detachment and attachment rates of a selected event, $K^-_{ev,i}$ and $K^+_{ev,i}$ respectively, is given by:

$$\frac{K^-_{ev,i}}{K^+_{ev,i}} = \exp\left(-\frac{\Delta\tilde{F}_{ev,i}}{\mathcal{R}T}\right) \tag{10}$$

with $\mathcal{R}$ the gas constant. After substitution of Eqs. (7)–(9) we obtain:

$$\begin{aligned} K^-_{ev,i} &= K^+_{ev,i}\exp\left(-\beta\Delta\tilde{F}_{ev}\right) \\ &= K^+_{ev,i}\exp\left(\frac{\alpha_{ii}}{\theta_i} - \frac{n_1\alpha_{i1} + n_2\alpha_{i2}}{3\theta}\right) \end{aligned} \tag{11}$$

where we have defined the dimensionless energies:

$$\alpha_{ij} = \frac{3\phi_{ij}}{\mathcal{R}T_2} \qquad (i, j = 1, 2) \tag{12}$$

and temperatures:

$$\theta = \frac{T}{T_2} \quad \text{and} \quad \theta_i = \frac{T_i}{T_2} \tag{13}$$

implying $\Theta_2 = 1$. Component 2 is taken to be the component with the highest melting temperature, so that $\Theta_1 \leq 1$. Commonly it is assumed that the attachment rate $K^+_{ev,i}$ is a liquid phase property, and is independent of the type of site, as characterized by the number of bonds formed. We will adopt this assumption defining $K^+_{ev,i} = K^+_i$. So the attachment rate for particles of type i is given by $K^+_i x^l_i$ for any type of surface site, where x^l_i is the mole fraction of component i in the liquid phase.

Summarizing, the MC model parameters are $\alpha_{ii} = \Delta U_i/\mathcal{R}T_2$ ($i = 1, 2$), $\alpha^{\mathrm{exc}} = \mathcal{U}^{s,\mathrm{exc}}_0/(\mathcal{R}T_2)$, Θ_1, the liquid composition $x^l_2 = 1 - x^l_1$ and the relative temperature θ. Actually, in the following we will rather use the undercooling $\Delta\Theta = \Theta - \Theta_{eq}$ to fix the temperature, where $\Theta_{eq} = T_{eq}/T_2$ is the dimensionless equilibrium temperature, which can be calculated for the given thermodynamic properties of the system.

In the MC simulations each configuration is represented by a 3D integer matrix $H(ix, iy, iz)$ for integer arguments ix, iy and iz. For each site (ix, iy, iz), with $0 < ix \leq N_x$, $0 < iy \leq N_y$ and $0 < iz \leq N_z$, $H(ix, iy, iz)$ has the value 0, 1 and 2 indicating a site not occupied by a solid particle and sites occupied by a solid particle 1 and 2 respectively. For a given set of input parameters many cycles of moves are performed. One cycle is $N_x N_y$ moves. One move is characterized by selecting randomly a surface position (ix, iy), followed by either the removal of the particle at the selected position, adding a new particle of type 1 or 2 on top of it, or no change at all according to the appropriately normalized probabilities for these events and decided by pulling a random number between 0 and 1.

For our MC simulations presented below a surface of dimensions $N_x \times N_y = 50 \times 50$ was used, containing a single step realized by an appropriate shift in the periodic boundary conditions. The step was employed to avoid the very long simulation times required for 2-dimensional nucleation in the non-roughened limit, i.e. for large interaction parameters α_{ii}.

3. Analytical models

3.1. Linear kinetic segregation model

The linear kinetic segregation (LKS) model is based on linear non-equilibrium thermodynamics applied to the

difference in bulk chemical potentials, i.e. neglecting the details of the growth kinetics at the surface. It assumes that the flux of each component i (=1, 2) from the liquid to the solid phase, J_i^+, and the reverse flux, J_i^-, are related by:

$$\frac{J_i^+}{J_i^-} = \exp\left(\frac{\Delta\mu_i}{\mathcal{R}T}\right) \tag{14}$$

where $\Delta\mu_i = \mu_i^l - \mu_i^s$ is the difference between the chemical potential of component i in the liquid phase, μ_i^l, and that of the growing solid phase, μ_i^s. As derived previously [27], this gives rise to a net flux of component i, $R_i = J_i^+ - J_i^-$, of the form:

$$R_i = N_k K_i^+ \left(x_i^l - x_{i,eq}^l\right) = N_k K_i \sigma_i \tag{15}$$

where $\sigma_i = x_i^l - x_{i,eq}^l$ is the absolute supersaturation of component i and where we included an additional proportionality constant N_k, defined as the average number of kink sites per unit surface area, and where $x_{i,eq}^l$ is specified below. Kink sites (see Fig. 1) play a crucial role in crystal growth. Referring to the Kossel model, particles at a kink site have three bonds and start to become well bonded to the crystal, unlike the sites with 1 or 2 bonds, from which an already adsorbed particle can easily dissolve again. The concept and meaning of kink sites is transferable to other lattices as well. It has been shown that the growth rate is in good approximation proportional to N_k [28]. According to Eq. (15) the composition of the growing solid phase, $x_2^s (=1-x_1^s)$, is determined through:

$$\frac{x_1^s}{x_2^s} = \frac{R_1}{R_2} = \frac{K_1^+\sigma_1}{K_2^+\sigma_2} = \frac{K_1^+\left(x_1^l - x_{1,eq}^l\right)}{K_2^+\left(x_2^l - x_{2,eq}^l\right)}. \tag{16}$$

In Eqs. (15) and (16), $x_{i,eq}^l$ is the equilibrium mole fraction of component i in the liquid phase with respect to the growing solid phase of composition x_2^s to be determined. For the systems specified in the previous section, $x_{i,eq}^l$ is given by:

$$x_{i,eq}^l = \gamma_i^s x_i^s \exp\left[\frac{\Delta U_i \Delta T_i}{\mathcal{R}T_i T}\right] \tag{17}$$

where $\Delta T = T - T_i$ and γ_i^s is the activity coefficient of component i in the growing solid phase. The activity coefficients, are related to the excess free energy by:

$$\gamma_1^s = \exp\left((x_2^s)^2 \frac{\mathcal{U}_0^{s,\mathrm{exc}}}{\mathcal{R}T}\right) \quad \text{and} \quad \gamma_2^s = \exp\left((x_1^s)^2 \frac{\mathcal{U}_0^{s,\mathrm{exc}}}{\mathcal{R}T}\right). \tag{18}$$

We note that equilibrium according to the LKS model, occurring at the temperature yielding $R_1 = R_2 = 0$, is equivalent to thermodynamic equilibrium.

For systems with a tendency to phase separation the solution of Eq. (16), including Eqs. (17) and (18), can have more than one solution. In Ref. [4] it was shown that Eq. (16) can be derived as the steady state solution of a first order differential equation and that the physically relevant solution has to fulfill the stability criterion for a stable steady state solution, being:

$$\frac{\mathrm{d}}{\mathrm{d}x_2^s}\left(R_2 - x_2^s R\right) < 0 \tag{19}$$

where $R = R_1 + R_2$ is the total growth rate. In addition, the individual growth rates have to be positive, i.e. $R_1 \geq 0$ and $R_2 \geq 0$.

Writing $\Delta U_i = \alpha_i \mathcal{R}T_2$, $\mathcal{U}_0^{s,\mathrm{exc}} = \alpha^{\mathrm{exc}}\mathcal{R}T_2$, and using Eq. (13), the expressions (17) and (18) are readily expressed in terms of the dimensionless parameters α_{ii} $(i = 1, 2)$, α^{exc}, Θ_1 and Θ, allowing a direct comparison with the MC simulation model.

3.2. Mean field kink site kinetic segregation model

The mean field kink site kinetic segregation (MFKKS) model is more kinetic than the LKS model, by including to some extent the growth kinetics at the surface. Actually, it is based on the kinetic incorporation rates of the components at kink sites permitting the composition at the kink site to be different from that of the bulk solid phase.

Thinking of the Monte Carlo model, we approximate the net incorporation rate of component i by:

$$R_i = N_k(K_i^+ x_i^l - \tilde{K}_i^- x_i^{sk}) \tag{20}$$

where x_i^{sk} is the average mole fraction of component i at kink sites and where $\tilde{K}_i^-$ is the average detachment rate of a particle i at a kink site. Then, similar to the LKS model, the growth composition follows from:

$$\frac{x_1^s}{x_2^s} = \frac{K_1^+ x_1^l - \tilde{K}_1^- x_1^{sk}}{K_2^+ x_2^l - \tilde{K}_2^- x_2^{sk}}. \tag{21}$$

In the MFKKS model we assume a mean field distribution of neighbours for the particle at the kink site, implying:

$$\tilde{K}_i^- = \sum_{j,k,l=1}^{2} x_j^s x_k^s x_l^s K_{ijkl}^- \tag{22}$$

where K_{ijkl}^- is the detachment rate of a particle i from a kink site with neighbours of type j, k and l along the step, on the terrace and down in the bulk respectively. So the compositions at each of these three neighbour sites are assumed to be equal to the bulk composition. Instead, the time average composition at the kink site itself, x_i^{sk}, is permitted to be different. Along a straight step, removal of a kink site particle will generally generate another kink site particle. This consideration brings us to the following expression for the variation in time of x_1^{sk}:

$$\frac{\mathrm{d}x_1^{sk}}{\mathrm{d}t} = K_1^+ x_1^l x_2^{sk} - K_2^+ x_2^l x_1^{sk} + \tilde{K}_{21}^- x_2^{sk} x_1^s - \tilde{K}_{12}^- x_1^{sk} x_2^s \tag{23}$$

where $\tilde{K}_{ij}^-$ $(i \neq j)$ is the average detachment probability for a kink particle of type i with a neighbour of type j along the step, which is assumed to become a kink particle itself after removal of its neighbour at the kink site. Within the MF approximation it reads:

$$\tilde{K}_{ij}^- = \sum_{k,l=1}^{2} x_k^s x_l^s K_{ijkl}^-. \tag{24}$$

An equation similar to Eq. (23) holds for component 2 but is not independent due to stoichiometry. Assuming steady state growth x_i^{sk} is constant, i.e. $\mathrm{d}x_i^{sk}/\mathrm{d}t = 0$, and Eq. (23) leads to:

$$x_1^{sk} = \frac{K_1^+ x_1^l + \tilde{K}_{21}^- x_1^s}{K_1^+ x_1^l + K_2^+ x_2^l + \tilde{K}_{21}^- x_1^s + \tilde{K}_{12}^- x_2^s} \tag{25}$$

while $x_2^{sk} = 1 - x_1^{sk}$. Eq. (25), including Eq. (24), expresses the kink composition as a function of the bulk composition of the growing solid phase, i.e. $x_i^{sk} = x_i^{sk}(x_2^s)$, so that Eq. (21), after substitution of Eqs. (22) and (25), and using $x_1^s = 1 - x_2^s$ becomes an equation with only one variable, x_2^s, which can be solved numerically without problems. We note that, in the above derivation of the kink site composition, surface diffusion has been neglected, which is reasonable for growth from the liquid phase.

We note that the equilibrium temperature according to the MFKKS model, i.e. the temperature at which the growth rate in Eq. (20) vanishes for $i = 1, 2$, can be different from the thermodynamic equilibrium temperature.

4. Kinetic phase diagrams

4.1. Confrontation

Each of the models described in the previous sections enable the determination of kinetic phase diagrams KPDs, giving the composition of the growing solid phase for liquid compositions along a liquidus line at a given undercooling $\Delta\Theta$. In this section we will compare the KPDs according to the analytical models with those from the MC simulations for systems with zero or relatively small excess energy. For all the calculations presented here and in Section 5, the kinetic constants are taken equal to each other, i.e. $K_1^+ = K_2^+$, as a reasonable assumption for isomorphous components.

Fig. 2 shows KPDs, and also the equilibrium phase diagrams, for two systems and different undercoolings. For the system corresponding to the graphs on the left the system parameters are $\alpha_{11} = \alpha_{22} = 6.5$, $\alpha^{\mathrm{exc}} = 0.5$ and $\Theta_1 = 0.9$, while for the system corresponding to the graphs on the right they are $\alpha_{11} = 6.0$, $\alpha_{22} = 7.0$, $\alpha^{\mathrm{exc}} = 0.5$ and $\Theta_1 = 0.9$. The here used values for the pure component parameters α_{ii} $(i = 1, 2)$ are typical for e.g. single aromatic molecular systems. The indicated undercoolings $\Delta\Theta$ are with respect to the thermodynamic temperature of the thermodynamic equilibrium temperature Θ_{eq}, which is equal to that of the LKS model. For the first system the KPDs according to the LKS model and the MFKKS model are almost equal and agree very well with the results of the MC simulation model. For the second system the LKS model gives good agreement with the MC model near equilibrium while the MFKKS model gives a better agreement at larger undercooling. The MFKKS model is not consistent with the equilibrium phase diagram. Instead, the MC simulations reproduce the equilibrium phase diagram quite well, with a vanishing growth rate for $\Delta\Theta \to 0$. The equilibrium phase diagram according to the MFKKS model (dotted lines in graph (d)) yields a lower equilibrium

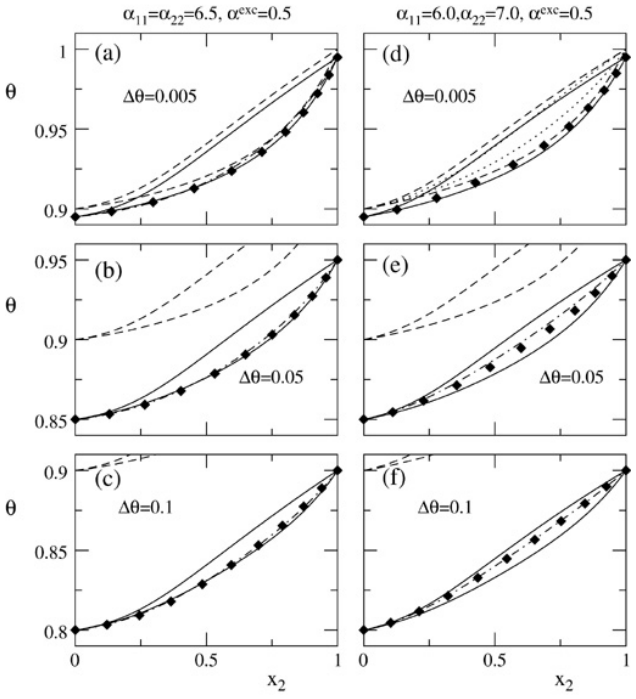

Fig. 2. Kinetic phase diagrams according to the LKS model (full line) and the MFKKS model (dotted–dashed lines), compared with the results from MC simulations (symbols) based on the isotropic binary Kossel model for three relative undercoolings $\Delta\Theta$ as indicated in the graphs. The graphs on the left side are the results for system parameters equal to $\alpha_{11} = \alpha_{22} = 6.5$, $\alpha^{\mathrm{exc}} = 0.5$ and $\Theta_1 = 0.9$, those on the right side are for $\alpha_{11} = 6.0$, $\alpha_{22} = 7.0$, $\alpha^{\mathrm{exc}} = 0.5$ and $\Theta_1 = 0.9$. The equilibrium phase diagrams is given by the dashed lines. The dotted lines in graph (d) give the equilibrium phase diagram according to the MFKKS model.

temperature and a too large solid phase mixing. We checked that these differences also occur for systems with zero excess energy. Due to them, the KPD for $\Delta\Theta = 0.005$ according to the MFKKS model is not given in graph (d), since $\Theta_{eq} - \Delta\Theta$ is slightly larger than the equilibrium temperature of the MFKKS model for a certain range of liquid compositions, implying a negative growth rate.

The mentioned difference in the results for the two systems appears to be typical in the sense that when the bond energies between like particles are equal (or very similar), i.e. when $\alpha_{11} \simeq \alpha_{22}$, then the LKS model agrees well with the MC model, both near equilibrium, approaching the equilibrium phase diagram, and at large undercooling, as long as the excess energy is not 'large', e.g. not so large that phase separation starts to occur. For the case $\alpha_{11} = \alpha_{22}$ and zero excess energy the results of the LKS model and the MFKKS model are exactly the same, which can be shown rigorously, and agree perfectly with the MC simulation results. In that case the kink composition is equal to the bulk composition. Instead when α_{11} is different from α_{22}, the LKS gives a good description near equilibrium, but deviations from the MC results start to occur at large undercooling, while the performance of the MFFKS model is the opposite.

For systems with larger melting entropies, i.e. larger α_{ii}, such as n-alkanes, fats, multiple aromatic molecular systems, etc., and a relatively large difference between α_{11} and α_{22} the

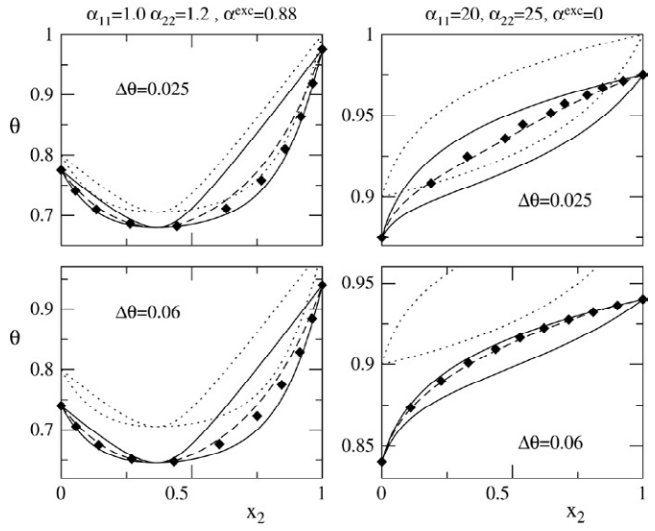

Fig. 3. Confrontation of the kinetic phase diagrams according to the LKS model (full lines) and the combined LKS-MFKKS model (dashed lines) with the results from MC simulations for two model systems and two relative undercoolings $\Delta\Theta$. The model parameters are indicated at the top for the left and right graphs respectively. The dotted lines give the equilibrium phase diagrams.

discrepancy between the LKS model and the MC simulations becomes much more significant. This is illustrated in the graphs at the right side of Fig. 3 for a system with $\alpha_{11} = 20.0$, $\alpha_{22} = 25.0$ and $\alpha^{\text{exc}} = 0$. For a system with small α_{ij}-parameters, such as metal systems, the differences remain small, even for relatively large excess parameters, as demonstrated in the graphs on the left side of Fig. 3. In this figure the dashed lines, showing a good overall agreement with the MC results, represent the results of a model which is a combination of the LKS model and the MFKKS model, as described hereafter.

4.2. Combined analytical model

The results in the previous section prompt us to the construction of an analytical model which tends to the LKS model for small undercooling and smoothly switches to the MFKKS for increasing undercooling. Therefore we propose the following combined LKS-MFKKS model.

For the combined model we write the growth rate of an individual component as a linear combination of those according to the LKS model and that according to the MFKKS model as:

$$\begin{aligned} R_i &= (1-S)R_i^{\text{LKS}} + SR_i^{\text{MF}} \\ &= N_k(K_i^+ x_i^l - (1-S)K_i^+ x_{i,eq}^l - S\tilde{K}_i^- x_i^{sk}) \end{aligned} \tag{26}$$

where $S = S(\Delta\Theta)$ is a smooth switch function depending on $\Delta\Theta$, described below, R_i^{LKS} and R_i^{MF} are the growth rates according to the LKS model (Eq. (15)) respectively and the MFKKS model (Eq. (20)). Similar to the other models the composition of the growing solid phase follows then from:

$$\frac{x_1^s}{x_2^s} = \frac{(K_1^+ x_1^l - (1-S)K_1^+ x_{1,eq}^l - S\tilde{K}_1^- x_1^{sk})}{(K_2^+ x_2^l - (1-S)K_2^+ x_{2,eq}^l - S\tilde{K}_2^- x_2^{sk})}. \tag{27}$$

The switch function S is defined as:

$$S = \frac{\Delta\Theta^2}{\Delta\Theta^2 + q^2 + \epsilon} \tag{28}$$

where:

$$q = (q_0\Delta\Theta_{eq} - \Delta\Theta)^2\Theta(q_0\Delta\Theta_{eq} - \Delta\Theta) \tag{29}$$

where q_0 and ϵ are two parameters, $\Theta(x)$ is the Heaviside step function, and $\Delta\Theta_{eq}$ is the difference in the equilibrium temperature according to the LKS model, Θ_{eq}^{LKS}, and the MFKKS model, Θ_{eq}^{MF}, i.e.:

$$\Delta\Theta_{eq} = \Theta_{eq}^{\text{LKS}} - \Theta_{eq}^{\text{MF}}. \tag{30}$$

Clearly, for $\Delta\Theta = 0$, $S = 0$ and the combined model becomes equal to the LKS model, whereas for large $\Delta\Theta$, S tends to one and the MFKKS model becomes dominant. The term q^2 in the denominator of Eq. (28) is added to make sure that the combined model yields a solution with a positive growth rate for any temperature below the thermodynamic equilibrium temperature $\Theta_{eq} = \Theta_{eq}^{\text{LKS}}$. We note that usually $\Theta_{eq}^{\text{MF}} < \Theta_{eq}^{\text{LKS}}$, so that a too fast switch to the MFKKS model may lead to a situation where the actual temperature is above the equilibrium temperature of the combined model. The values of the parameters are $q_0 = 4/3$ and $\epsilon = 2.5 \times 10^{-5}$. These values were chosen such that the switch is smooth and that a rapid switch to the MFKKS model is achieved below the temperature $\Theta_{eq}^{\text{LKS}} - q_0\Delta\Theta_{eq}$. Basically, these parameters imply a rapid switch to the MFKKS in most cases, since $\Delta\Theta_{eq}$ is usually rather small. This rapid switch was inspired by the MC results, which are well predicted by the MFKKS model already at rather small undercooling, especially for large interaction parameters α_{ii}. This is demonstrated by the KPDs graphs at the right of Fig. 3. At $\Delta T = 0.025$ the LKS-MFKKS model is in good agreement with the MC results. We checked that in this case the LKS-MFKKS model is already very close to the MFKKS model.

5. Kinetic phase separation domains

For large interaction parameters α_{ii} $(i = 1, 2)$ and large excess energy, yielding eutectic or peritectic equilibrium phase diagrams, the analytical kinetic models of Section 3 can give two stable steady state solutions. The KPDs for such systems then have two branches, corresponding to growing solid phases rich in component 1 and 2, respectively. For the LKS model this was shown in [5]. Qualitatively, the MFKKS shows the same behaviour. Typically, this so-called kinetic phase separation occurs in a certain domain of the phase diagrams below the equilibrium liquidus. We will denote such a domain as a kinetic phase separation domain (KPSD). Examples of KPSDs, calculated according to the various analytical models, are shown in Fig. 4 for $\alpha_{11} = \alpha_{22} = 20$ and for two different values of the excess energy parameter, namely $\alpha_{\text{exc}} = 4$ and $\alpha_{\text{exc}} = 6$, both yielding eutectic equilibrium phase diagrams. The KPSDs are indicated by the shaded areas. As expected, for small undercooling, kinetic phase separation only occurs

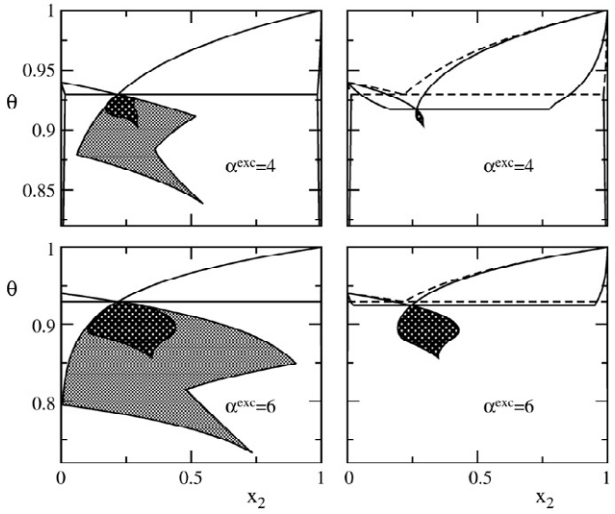

Fig. 4. Kinetic phase separation domains (KPSDs) according to the LKS model (graphs on the left, light-shaded areas), the combined LKS-MFKKS model (graphs on the left, dark-shaded areas) and the MFKKS model (graphs on the right, dark-shaded areas) for model systems with $\Theta_1 = 0.94$, $\alpha_{11} = \alpha_{22} = 20$ and for excess values $\alpha^{\text{exc}} = 4$ (upper graphs) and $\alpha^{\text{exc}} = 6$ (lower graphs).

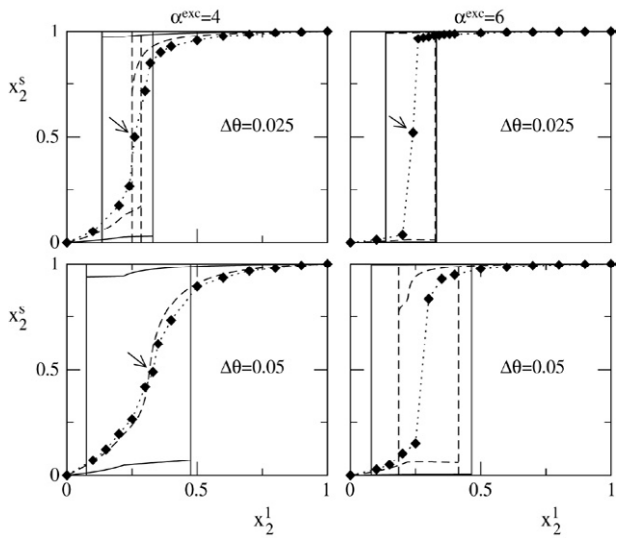

Fig. 5. The solid phase composition(s) x_2^s as a function of the liquid composition x_1^l according to the LKS model (full lines) and the LKS-MFKKS model (dashed lines) for two eutectic systems, parametrized by $\Theta_1 = 0.94$ and $\alpha_{11} = \alpha_{22} = 20$, and excess parameters $\alpha^{\text{exc}} = 4.0$ (graphs on the left) and $\alpha^{\text{exc}} = 6.0$ (graphs on the right). Within the range of liquid compositions marked by the two vertical lines, the models predict kinetic phase separation, hence two solid phase compositions, except for the case with $\alpha^{\text{exc}} = 4.0$ and $\Delta\Theta = 0.05$, where the LKS-MFKKS predict one growing solid phase for all liquid compositions. The symbols, accompanied by a dotted line for guiding the eye, give the average solid phase compositions resulting from MC simulations.

near the eutectic liquid phase composition. For increasing undercooling the range of liquid compositions yielding kinetic phase separation first becomes larger but then it starts to decrease and finally vanishes. The larger the excess energy, the lower is the temperature where kinetic phase separation vanishes, and the larger is the KPSD. This holds for all models, but the KPSDs for the MFKKS and the combined LKS-MFKKS are much smaller than those according to the LKS model, due the enhanced tendency to mixing according to the MFFKS model. We note that also here the equilibrium liquidus according to the MFKKS model lies below that of the LKS model and the combined LKS-MFKKS model, for which the equilibrium temperatures are equal by construction.

Fig. 5 shows a comparison between the analytical models and the results from MC simulations for the systems of Fig. 4. Simulations were done for a set of liquid compositions at constant $\Delta\Theta$ below the equilibrium temperature, for $\Delta\Theta = 0.025$ and 0.05. Fig. 5 shows the resulting average compositions (symbols) of the solid phase as a function of the liquid composition. Depending on the liquid composition the analytical models yield one or two steady state solutions. The range of liquid compositions with two steady state solutions is marked by two vertical lines. Within this range there are two solid phase composition branches. In the regions with only one steady state, the LKS-MFKKS model (dashed lines) agrees rather well with MC results. Within the two steady state regions of the LKS-MFKKS model the MC results switch from 1-rich to a 2-rich solid phase for liquid compositions from the left to the right vertical dashed line, hence within the phase separation domain according to the LKS-MFKKS model. Taking into consideration that the solid phase composition from the MC simulations is an average composition, this is precisely what one would expect. In one case, namely for $\alpha^{\text{exc}} = 4$ and $\Delta T = 0.05$, the LKS-MFKKS model predicts no phase separation, again in agreement with the MC results. Thus, also for a strongly phase separating system the LKS-MFKKS reproduces quite well the trends in the segregation. Instead, the LKS model starts to deviate considerably from the MC results for such systems. It predicts a too strong segregation of the components and the phase separation domains are too large.

In order to get a better understanding of the connection between the results from the analytical models and the MC simulations at conditions within the phase separation domains for the system of Fig. 5, we inspected the grown Kossel crystals with solid phase mole fraction close to 0.5. In Fig. 6, cross-sections parallel to the growth direction of three different simulated crystals, with solid phase compositions around 0.5 as specified in the figure caption, are shown. Fig. 6(a) shows the crystal cross-section for $\alpha^{\text{exc}} = 4$ and $\Delta\Theta = 0.025$. According to both models phase separation should occur, but the phase separation domain for the MFKKS model is rather narrow in this case and the corresponding point of the MC simulation in Fig. 5 actually lies on the boundary of it. Fig. 6(b) highlights a point for $\alpha^{\text{exc}} = 4$ and $\Delta\Theta = 0.05$, where the MFKKS does not predict phase separation, in contrast to the LKS model. One can see that in this case the crystal is more mixed than that in Fig. 6(a). In the case of Fig. 6(a) one could speak of domain formation, but with small domain size. Thus, the MC results are more or less in agreement with the predictions of the LKS-MFKKS model, and not with those of the LKS model which predicts phase separation in the case of Fig. 6(b). Fig. 6(c), corresponding to a point for $\alpha^{\text{exc}} = 6$, $\Delta\Theta = 0.025$, shows phase separation, but with much larger domains. Here the observed phase separation is in agreement with both models.

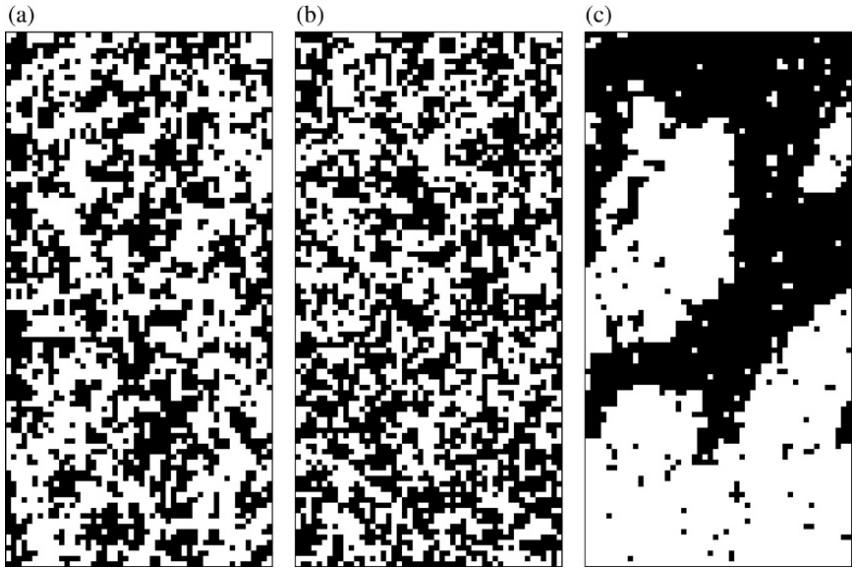

Fig. 6. Cross sections parallel to the growth direction of binary Kossel crystals grown by MC simulation. The pictures are from simulations for (a) $\alpha^{\mathrm{exc}} = 4$, $\Delta\Theta = 0.025$ and $x_2^l = 0.26$ giving $x_2^s = 0.50$, for (b) $\alpha^{\mathrm{exc}} = 4$, $\Delta\Theta = 0.05$ and $x_2^l = 0.33$ giving $x_2^s = 0.49$; and for (c) $\alpha^{\mathrm{exc}} = 6$, $\Delta\Theta = 0.025$ and $x_2^l = 0.24$ giving $x_2^s = 0.52$, indicated by the arrows in Fig. 5.

However, again, the MC results for larger undercooling for this system are in contrast with the LKS model, while the LKS-MFKKS model remains in agreement with MC simulations.

6. Conclusions and perspectives

We have investigated kinetic segregation occurring during crystallization of binary mixtures from the liquid phase at isothermal conditions on the basis of a Monte Carlo (MC) simulation model and analytical models. One of the analytical models, the linear kinetic segregation (LKS) model, was presented previously [4,27], and has hereby been tested by comparing it with the results from the MC model, which we have taken as reference. Close to equilibrium, the LKS model reproduces well the MC results, as could be expected since it is based on linear non-equilibrium thermodynamics, which should be a good approximation near equilibrium. Equilibrium according to the LKS model coincides with thermodynamic equilibrium. This is an intrinsic property of the LKS model. At larger undercooling the LKS model still gives a reasonable approximation in certain cases, namely when the bond energies are small (e.g. for metal systems), or when the bond energies between like particles are not 'too' different and the excess energy is 'small', e.g. for well mixing systems. For other cases the LKS model can deviate considerably from the MC results. Instead, another, new analytical model, which is based on the growth kinetics at kink sites, assuming a mean field environment for the particle at the kink site, gives a good agreement with the MC results at moderate and large undercooling for arbitrary system parameters (or at least for a much wider domain in the parameter space). We denote the new model as the mean field kink site kinetic segregation (MFKKS) model. The good agreement of the MFKKS model with the MC results at moderate and large undercooling also holds for phase separating systems. However, it generally does not reproduce the equilibrium phase diagram for conditions close to equilibrium. Therefore, we have constructed a third model which is a combination of the LKS model and MFKKS model, the LKS-MFKKS model. Close to equilibrium the LKS-MFKKS is (almost equal to) the LKS model, but for increasing undercooling the LKS-MFKKS model becomes rapidly equivalent with the MFKKS model. Thus, the LKS-MFKKS model provides a good description for the entire range of undercoolings, and matches with thermodynamic equilibrium for zero undercooling. This makes it a suitable model to be incorporated in continuum models for the crystallisation of mixtures, like phase field models.

Here we have not included the effects of mass and heat transport in the liquid phase, which are both coupled to the segregation at the growth interface and which can be expected to play an important role at large undercooling. Previously, we have developed an effective segregation model based on the LKS model, including the coupling with liquid phase diffusion of both mass and heat [9]. This extension can be applied straightforwardly to the LKS-MFKKS model as well.

Currently we are extending the binary Kossel model for the case with anisotropic binding energies, which would be an important step forward towards reality for many systems, in particular molecular systems. It remains to be seen whether such an anisotropy will change the MC results for equal total melting energies and excess energy. One could expect dependence on the orientation of the growth surface in that case. The LKS model cannot deal with anisotropy, but the LKS-MFKKS model can be extended to the anisotropic case. Then, another step forward towards reality we planned is to extend the MC model to more realistic crystal structures, as characterized by the topology of the bonds. This would be a binary or a multi-component extension of the pure component crystal growth MC program MONTY [29].

Acknowledgment

This work has been sponsored by Stichting Technische Wetenschappen (STW), The Netherlands.

References

[1] P.A. Reynolds, Mol. Phys. 29 (1975) 519.
[2] M. Matovic, J.C. van Miltenburg, J.H. Los, J. Cryst. Growth 275 (2005) 211.
[3] M. Matovic, J.C. van Miltenburg, J.H. Los, CALPHAD (submitted for publication).
[4] J.H. Los, W.J.P. van Enckevort, E. Vlieg, E. Flöter, J. Phys. Chem. B 106 (2002) 7321.
[5] J.H. Los, W.J.P. van Enckevort, E. Vlieg, E. Flöter, F.G. Gandolfo, J. Phys. Chem. B 106 (2002) 7331.
[6] A.C.G. van Genderen, C.G. de Kruif, H.A.J. Oonk, Z. Phys. Chem. Neue Folge 107 (1977) 167.
[7] Z. Zbionski, J. Cryst. Growth 58 (1982) 335.
[8] J.A. Bouwstra, A.C.G. van Genderen, N. Brouwer, H.A.J. Oonk, Thermochim. Acta 38 (1980) 97.
[9] J.H. Los, M. Matovic, J. Phys. Chem. B 30 (2005) 14632.
[10] T.A. Cherepanova, J.P. van der Eerden, P. Bennema, J. Cryst. Growth 44 (1978) 537.
[11] T.A. Cherepanova, J.B. Dzelme, Cryst. Res. Technol. 16 (1981) 399.
[12] G.H. Gilmer, P. Bennema, J. Cryst. Growth 13 (1972) 148.
[13] G.H. Gilmer, P. Bennema, J. Appl. Phys. 43 (1972) 1347.
[14] H. Pfeiffer, Th. Klupsch, W. Haubenreisser, Microscopic Theory of Crystal Growth, Akademic Verlag, Berlin, 1989.
[15] P. Rudolph, Mater. Sci. Forum 276 (1998) 1.
[16] M.J. Aziz, J. Appl. Phys. 53 (1982) 1158.
[17] M.J. Aziz, J. Appl. Phys. Lett. 43 (1983) 552.
[18] K.A. Jackson, G.H. Gilmer, D.E. Temkin, Phys. Rev. Lett. 75 (1995) 2530.
[19] K.A. Jackson, K.M. Beatty, K.A. Gudgel, J. Cryst. Growth 271 (2004) 481.
[20] K.M. Beatty, K.A. Jackson, J. Cryst. Growth 174 (1997) 28.
[21] S.U. Campisano, G. Floti, P. Baeri, M.G. Grimaldi, E. Rimini, Appl. Phys. Lett. 37 (1980) 719.
[22] P. Baeri, J.M. Poate, S.U. Campisano, G. Floti, E. Rimini, A.G. Cullis, Appl. Phys. Lett. 37 (1980) 912.
[23] C.W. White, S.R. Wilson, B.R. Appleton, F.W. Young Jr., J. Appl. Phys. 51 (1980) 738.
[24] N. Matsumoto, M. Kitamura, J. Cryst. Growth 222 (2001) 667.
[25] N. Matsumoto, M. Kitamura, J. Cryst. Growth 237 (1) (2002) 51.
[26] M. Kitamura, N. Matsumoto, J. Cryst. Growth 260 (2004) 243.
[27] J.H. Los, E. Flöter, J. Phys. Chem. Chem. Phys. 1 (1999) 4251.
[28] J.P. van der Eerden, Handbook of Crystal Growth 1a, Chapter 6, 307: Crystal Growth Mechanisms, Elsevier, Amsterdam, 1993.
[29] S.X.M. Boerrigter, G.P.H. Josten, J. van de Streek, F.F.A. Hollander, J.H. Los, H.M. Cuppen, P. Bennema, H. Meekes, J. Phys. Chem. A 108 (2004) 5894.